

Toward Ka Band Acoustics: Lithium Niobate Asymmetrical Mode Piezoelectric MEMS Resonators

Yansong Yang, Ruochen Lu, Tomas Manzaneque, and Songbin Gong

Department of Electrical and Computer Engineering
University of Illinois at Urbana-Champaign
Urbana-Champaign, USA
yyang165@illinois.edu

Abstract— This work presents a new class of micro-electro-mechanical system (MEMS) resonators toward Ka band (26.5-40 GHz) for fifth-generation (5G) wireless communication. Resonant frequencies of 21.4 and 29.9 GHz have been achieved using the fifth and seventh order asymmetric (A5 and A7) Lamb-wave modes in a suspended Z-cut lithium niobate (LiNbO₃) thin film. The fabricated device has demonstrated an electromechanical coupling (k_t^2) of 1.5% and 0.94% and extracted mechanical Q s of 406 and 474 for A5 and A7 respectively. The quality factors are the highest reported for piezoelectric MEMS resonators operating at this frequency range. The demonstrated performance has shown the strong potential of LiNbO₃ asymmetric mode devices to meet the front-end filtering requirements of 5G.

Keywords—Ka Band; 5G wireless communications; Internet of Things; lithium niobate; asymmetrical modes; MEMS resonators

I. INTRODUCTION

Recently, due to the market demand for higher data rate for cellular phone applications, below 3 GHz spectrum has become increasingly crowded with little available spectrum for the expansion of fifth-generation (5G) wireless communication systems. As a result, Federal Communications Commission (FCC) has opened frequency bands 27.5-28.35 GHz and 37-40 GHz for licensed use, which overlaps with Ka band, for 5G mobile radio applications [1]. Several European and Asian countries have also planned portions of Ka band for the same purpose [2]. This expansion has sparked new technology development to overcome the remaining bottlenecks in accessing this portion of the spectrum. One key missing piece in beyond-24 GHz front-ends is high-performance and miniature filters that can be arrayed in a smart phone. At fourth-generation (4G) frequency ranges (<3 GHz), filters based on acoustic and MEMS resonators have been widely adopted. However, it remains challenging to scale these devices in frequency to meet 5G requirements.

The state-of-the-art acoustic resonators beyond 24 GHz resort to either the fundamental FBAR mode in a 100 nm thin AlN film or an overtone FBAR mode in a thicker AlN film [3] [4]. In either case, significant performance compromise has to be made in the process of scaling, which might lead to inadequate performance for 5G applications. For instance, a suspended 100 nm AlN thin film would produce a high thermal resistance to the surrounding. In addition, matching to system resistance (50 Ω) beyond 24 GHz requires small static capacitance ($C_0 < 150$ fF), which limit the size (length-width < 200 μm^2) of 100 nm thick

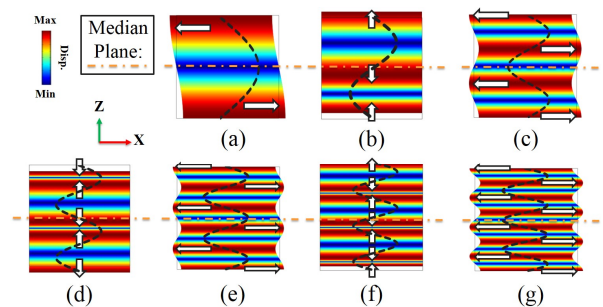


Figure 1: Displacement mode shapes of the (a) first-order (A1), (b) second-order (A2), (c) third-order (A3), (d) fourth-order (A4), (e) fifth-order (A5), (f) sixth-order (A6), and (g) seventh-order (A7) asymmetric modes. The arrows denote the displacement directions. The stress field for each mode order is plotted in black dashed line.

FBAR. All these limitations lower the power handling and increase the thermal nonlinearity of the resonator [5]. On the other hand, overtone operations, despite providing better power handling via a thicker film, would lead to diminished electromechanical coupling (k_t^2) as it will be discussed in this paper.

To overcome these limitations, one alternative is to select an acoustic wave mode in a material that features much higher electromechanical coupling than AlN FBARs so that frequency scaling toward Ka Band based on higher orders can still produce reasonable k_t^2 to meet 5G bandwidth requirement. It is also preferable that the mode has a large acoustic velocity so that scaling would not reduce the feature size to the extent that limits power handling. Recently, several modes (S0, SH0, and A1) have been demonstrated in LiNbO₃ with high coupling factors [6-10]. Among these wave modes, A1 Lamb wave mode has the highest phase velocity, and has been demonstrated with very large k_t^2 and Q s simultaneously in Z-cut LiNbO₃ ($k_t^2=28\%$ and $Q=500$ at 5 GHz), and in Y-cut LiNbO₃ ($k_t^2=6.3\%$ and $Q=5341$ at 1.7 GHz) [9] [10]. Therefore, A1 mode devices are being considered as an alternative resonator technology for sub-6 GHz applications. However, the higher order asymmetrical modes have not yet been explored for scaling the resonant frequency beyond 6 GHz.

In this work, we aim to extend asymmetrical Lamb wave modes in Z-cut LiNbO₃ to higher orders for beyond-24 GHz applications. We first investigate the excitation of asymmetric modes of various orders. More specifically, the dependence of electromechanical coupling factor on mode order and resonant

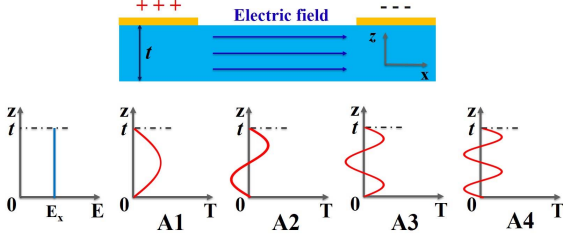


Figure 2: Distribution of electrical and stress fields of A1, A2, A3, and A4 modes.

frequency is studied with both analytical and finite element methods. Based on these studies, a film thickness of 400 nm is chosen to support the fifth and seventh order asymmetric (A5 and A7) modes to move up and reach Ka band. The fabricated device is measured with k_r^2 of 1.5% and 0.94% and extracted mechanical Q_s of 406 and 474, at 21.4 GHz and 29.9 GHz for A5 and A7 modes, respectively.

II. ASYMMETRIC LAMB WAVE MODES IN LITHIUM NIOBATE THIN FILM

Asymmetric modes are a class of Lamb-wave modes characterized by their particular anti-symmetry about the median plane of the plate. In other words, they have equal vertical displacement components but opposite longitudinal components on different sides of the median plane [11]. To visualize the displacement mode shapes of asymmetric modes of various orders, Comsol finite element analysis (FEA) is used to simulate the eigen modes in a 2D LiNbO₃ slab with free top and bottom surfaces and periodic boundaries in the lateral direction (Fig. 1). Various order modes from the first (A1) to seventh (A7) are shown with a mode order denoting the number of half-wavelength periodicities in the vertical direction. Clearly, overmoding a slab with a fixed thickness would yield a higher resonant frequency, provided the intended higher order mode can somehow be excited in the LiNbO₃ slab with transducers.

The simplest transducers for such a purpose are interdigital electrodes that are patterned exclusively on top of a transferred LiNbO₃ thin film, as they have least fabrication complication. As demonstrated by several prior works on A-modes, top-only interdigital transducers (IDT) can effectively excite the A1 modes with lateral electric fields [9] [10]. However, electromechanical coupling to asymmetric modes with mode orders higher than A1 has not been well studied with top-only IDTs. To understand the excitation of higher-order A-modes with IDT, magnitudes of the stress standing waves for different order modes are depicted in Fig. 1 and 2. As seen in Fig. 2, we simplify the E-field introduced by IDTs as laterally polarized with a uniform magnitude across the thickness of the plate. Thus, the integration of stress and the lateral electrical fields, which describes the mutual energy between the electrical and mechanical domains [12], vanishes for even-order modes and leads to zero electromechanical coupling to these modes (according to Berlincourt's definition of k_r^2). On the other hand, odd order modes can be excited due to non-zero integral of mutual energy. For the purpose of frequency scaling to Ka band, our overmoding approach will focus on the odd order modes with the simple top-only IDTs.

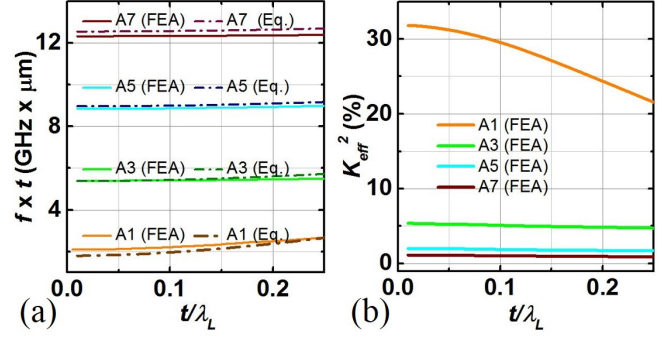


Figure 3: (a) Calculated and simulated $f \times t$ product and (b) Simulated effective electromechanical coupling factor of A1, A3, A5, and A7 modes vs. the ratios of film thickness to longitudinal wavelength (t/λ_L).

To more precisely predict the resonant frequency and electromechanical coupling of a higher odd order A-mode, we have to resort a more refined model that treats the cross-section of the resonator as a two-dimensional cavity, instead of an infinitely long slab seen in Fig. 1 [11]. The resonant frequency of an odd order mode in a two-dimensional cavity with thickness of t and length of l is given by

$$f_0^{mn} = \sqrt{\left(\frac{mv_t}{2t}\right)^2 + \left(\frac{nv_L}{2l}\right)^2} \quad (1)$$

where m and n are the mode orders in the vertical (z -axis) and longitudinal (x -axis) directions, respectively. v_t and v_L are the acoustic phase velocities in the vertical and longitudinal directions. The asymmetric modes of interest in this work have a longitudinal mode order n of 1 with a vertical mode order m that takes a value among 1, 3, 5 and 7. Note that Eq. 1 assumes the lateral boundaries are mechanically free, the same as the top and bottom surfaces. This assumption will be revisited later. Eq. 1 also implies that any composite mode of order f_0^{mn} with n taking an odd value larger than 1 can emerge as a spurious mode near the intended mode f_0^{m1} . Such a phenomenon has been observed for other high coupling resonators with a 2D nature [13] [14].

For modes with $n=1$, l is equal to half of the longitudinal wavelength ($\lambda_L/2$). Thus, Eq. 1 can be re-written as:

$$f_0^{m1} = \frac{v_L}{2t} \sqrt{(\alpha m)^2 + \left(2 \frac{t}{\lambda_L}\right)^2} \quad (2)$$

where α is the ratio between the velocity of vertical and longitudinal directions:

$$\alpha = \sqrt{c_{55}/c_{11}} \quad (3)$$

To validate the two-dimensional analysis, Comsol-based FEA is used to calculate the frequency variation of each odd-order asymmetrical mode in a Z-cut LiNbO₃ thin film. Fig. 3 (a) shows the simulated and calculated frequency-thickness products ($f \times t$) as a function of the ratio of plate thickness to longitudinal wavelength (t/λ_L). The discrepancies between simulation and calculation are likely caused by several simplifications used in the calculation.

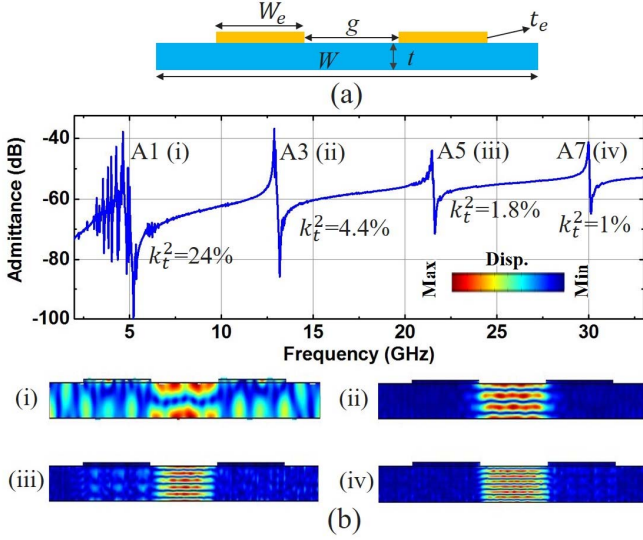


Figure 4: (a) Mocked-up view of designed asymmetric mode LiNbO₃ resonator. (b) Simulated response of a Z-cut LiNbO₃ A-mode resonator. Displacement mode shapes of (i)A1, (ii)A3, (iii)A5, and (iv)A7 are included.

TABLE I

Physical dimensions of the designed asymmetric mode resonator					
Electrode width, W_e	Device width, W	Electrode thickness, t_e	Film thickness, t	Spacing between electrodes, g	Total length, L
3 μm	13 μm	60 nm	400 nm	3 μm	100 μm

In addition to the resonant frequency, each mode is also characterized by an effective electromechanical coupling factor (k_{eff}^2) [15]:

$$k_{eff}^2 \approx \frac{e^2}{\epsilon^s c^E} \cdot k_{v,m}^2 \cdot k_{l,n}^2 \quad (4)$$

where e is the piezoelectric efficient, ϵ^s is the permittivity under constant strain, c^E is the stiffness under constant electric field. $k_{v,m}^2$ is a scaling factor capturing the dependence of k_{eff}^2 on the stress and electric field distributions of the m^{th} order mode in the vertical direction. Similarly, $k_{l,n}^2$ represents the dependence of k_{eff}^2 on the stress field distribution of n^{th} order mode in the longitudinal direction [11]. The expression of $k_{v,m}^2$, as part of the Berlincourt Formula, is given as:

$$k_{v,m}^2 = \frac{(\int E_x(z)u_x(z)dz)^2}{\int E_x^2(z)dz \cdot \int u_x^2(z)dz} \quad (5)$$

By using the simplified field distributions shown in Fig. 2 for integration, $k_{v,m}^2$ can be formulated as a function of mode order m :

$$k_{v,m}^2 = \frac{1}{m^2} \quad (6)$$

$k_{l,n}^2$ in Eq. 4 is dependent to the ratio between the vertical and longitudinal dimensions (t/λ_L), and typically increases with respect to m . Therefore, the lower bound for k_{eff}^2 of the m^{th} -order ($m > 1$) asymmetric mode is $1/m^2$ of k_{eff}^2 of the A1 mode.

To further understand the diminishing effect of overmoding on k_{eff}^2 (also the dispersive relationship between $k_{l,n}^2$ and t/λ_L), Comsol FEA is used to calculate the k_{eff}^2 as a function of t/λ_L .

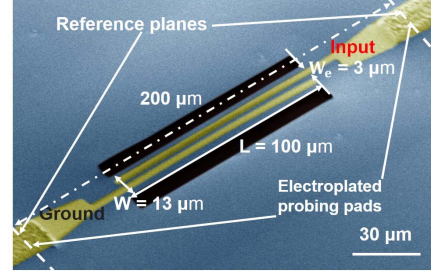


Figure 5: SEM image of the fabricated device.

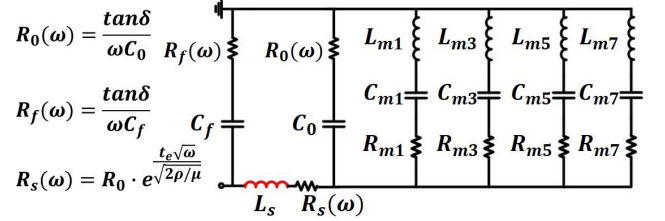


Figure 6: Multi-resonance equivalent MBVD circuit model with an added series inductor. $\tan\delta$ is the loss tangent of LiNbO₃, ρ is the resistivity of gold, and μ is the permeability of Au.

The relationship, shown in Fig. 3(b), indicates that overmoding into A3, A5, and A7 can still have meaningful k_{eff}^2 for 5G applications if it starts with a large k_{eff}^2 of 30%, which is attainable for A1 mode with a $t/\lambda_L < 0.1$.

Based on the above analyses (summarized in Fig. 3), we choose the thickness of the thin film to be 400 nm, and λ_L to be 6 μm so that the targeted A5 and A7 modes can be scaled toward Ka band with reasonably large k_{eff}^2 . t of 400 nm and λ_L of 6 μm are also deemed as a good tradeoff between having an adequately low t/λ_L and achieving a reasonably large static capacitance (C_0) for the resonator. Based on Fig. 3 (a), the A7 mode in such a cavity would yield a resonant frequency at 30 GHz.

III. DESIGN AND MODELING OF ASYMMETRIC MODE RESONATOR

To validate resonant characteristics and factor in the effects of electrodes, the resonator is simulated with 2D Comsol FEA. As shown in the cross-sectional mock-up in Fig. 4 (a), the device consists of a 2-electrode transducer on top of a mechanically suspended 400 nm thick Z-cut LiNbO₃ thin film. The two electrodes, connected to signal and ground respectively, induce lateral electric fields in the LiNbO₃ thin film, which subsequently excite the resonator into odd-order asymmetric mode vibration. 60 nm gold is used as the electrodes in the simulation. Gold is used for its good conductivity while thickness is kept low to avoid excess mass loading and shifting down the resonances. The design parameters are summarized in Table I. The Comsol simulated response is shown in Fig. 4 (b), including the displacement mode shape of each excited asymmetric mode. Different from fundamental Lamb waves (S0, A0), the higher order A-modes are confined between two electrodes, so the longitudinal cavity dimension is approximately the distance between adjacent electrodes. We already considered this effect in the design process by setting the distance between the electrodes to 3 μm ,

TABLE II
Key measured values (in bold symbols) and extracted parameters of the multi-resonance MBVD model

Order (m)	f_0	R_{mi}	C_{mi}	L_{mi}	$R_s(\omega)$	C_0	C_f	L_s	$\tan\delta$	Q_o	k_t^2	FoM	Extracted Mechanical Q_m
1	4.5 GHz	74 Ω	3.84 fF	319 nH	12.5 Ω	19.4 fF	13.5 fF	90 pH	0.07	118	24%	28.3	122
3	12.9 GHz	78 Ω	0.574 fF	267 nH	12.9 Ω					224	3.7 %	8.3	277
5	21.4 GHz	82 Ω	0.225 fF	247.3 nH	13.2 Ω					287	1.5 %	4.3	406
7	29.9 GHz	76 Ω	0.15 fF	192 nH	13.4 Ω					328	0.94%	3.1	474

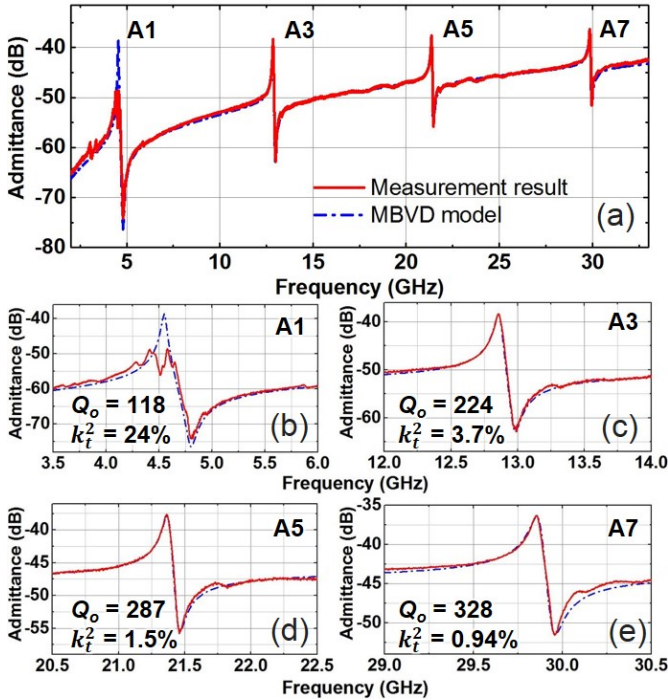


Figure 7: (a) Measured and multi-resonant equivalent MBVD circuit modeled response of an asymmetric mode LiNbO₃ resonator with zoomed-in view of (b) A1, (c) A3, (d) A5, and (e) A7 mode resonances.

half of the target λ_L value. This local confinement of displacement for A3, A5 and A7 modes is believed to be caused by the acoustic impedance mismatch between the metalized and unmetalized sections, which increases with respect to the mode order. Strictly speaking, Eq. 2 can no longer apply to calculating the resonances as such confinement does not have mechanical free boundaries assumed in the derivation of Eq. 2. Instead, complex reflection coefficients should be used to capture longitudinal boundaries. However, the tight confinement as seen in Fig. 4 leads to the belief that Eq. 2 could be still used for estimates of resonances with good accuracy.

Consistent with our theoretical analyses in Section II, FEA results show that only the odd-order modes are excited. The first four odd modes, A1, A3, A5 and A7, have resonant frequencies at 4.5, 12.8, 22, and 30 GHz respectively. The simulated effective electromechanical coupling factors for these modes are 24%, 4.4%, 1.8% and 1%, showing the theoretically predicted diminishing trend. It scales slightly better than $1/m^2$ due to the aforementioned dispersive relationship between $k_{t,n}^2$ and mode order, the simulated results on resonator k_t^2 are also on par with the predictions based on Eq. 4 and in Fig. 3(b).

IV. MEASUREMENTS AND DISCUSSIONS

To validate the analytical and modeling results, the designed Z-cut LiNbO₃ A-mode resonator was fabricated on a 400 nm-transferred Z-cut LiNbO₃ thin film following the process described in [9]. The fabricated device is shown in Fig. 5. 60 nm-Au is sputtered and lift-off as the top electrodes. The probing pads, also made of Au, are electroplated to 2.5 μm to reduce loss. To reduce the parasitic effect between the lead lines, a 200 μm pitch between probing pads is used. The fabricated device was characterized over a wide frequency range (up to 40 GHz) with a Keysight N5230A PNA-L network analyzer in dry air and at room temperature. A TRL calibration based on on-wafer standards is used to move the measurement reference planes to the positions as labeled in Fig. 5.

Similar to the simulation results in Fig. 4, the measurement results shown in Fig. 7(a) exhibit resonant frequencies at 4.5, 12.8, 21.4, and 29.9 GHz, corresponding to the anticipated A1, A3, A5, and A7 modes respectively. As expected, even-order asymmetric modes cannot be observed with this design. Among the first four odd-order asymmetric modes shown in Fig. 7(b-d), a higher order yields a higher measured overall quality factor, Q_o (including the effects of all loss mechanisms). The reason behind this phenomenon is still under investigation.

A multi-resonance modified Butterworth-Van Dyke (MBVD) model, in which each resonance is captured by a motional branch of R_m , L_m , and C_m , is used to interpret the measurement results. As shown in Fig. 6, an additional series inductor (L_s) is added to account for the non-negligible inductance of the electrode fingers at high frequencies. An additional resistor (R_s) is added to account for surface resistance of electrodes and bus lines, the value of which is dependent on frequency due to skin effects and calculated based on the equation shown in Fig. 6. To account for the parasitic effects, C_f and R_f are included as the feedthrough capacitance and loss in the substrate, respectively. An on-chip test structure consisting of only the bus lines was included in fabrication to measure the value of C_f . Except for the overall Q_o resonances, and C_f , other parameters in the multi-resonance MBVD model are extracted from measurements. By excluding the loss in the electrical domain, we can also extract the mechanical Q_m at these resonances from the MBVD model. It is worth noting that the A7 mode demonstrates a very high mechanical Q of 474 at 30 GHz. Q_m for other resonances, along with extracted k_t^2 of each mode and other key parameters of the MBVD models, are listed in Table II. As seen in Fig. 7, the response of the MBVD model excellently fits with measured admittance response, hence validating the parameter extraction. The effects of self-inductance and feedthrough capacitance have been de-embedded for the extracted k_t^2 values. The extracted k_t^2 values match the simulated results shown in Fig. 4, as well as

the analytical results in Fig. 3(b). The agreement thus confirms the effectiveness of our frequency scaling approach based on overmoding asymmetric modes.

The measured results herein have demonstrated the potential of higher-order A-modes for enabling Ka band acoustic resonators. A mechanical Q of 474, as demonstrated for A7, has already exceeded the state of the FBAR results [3]. Further Q enhancement has to rely on more sophisticated understanding the acoustic loss at this frequency range, as well as reducing dissipation in the electrical domain. To achieve a large k_t^2 and higher filter bandwidth at these frequencies, a thinner LiNbO₃ film may be adopted with our approach to scale the A5 mode to Ka band. This, however, will likely come at the cost of lower power handling and linearity.

V. CONCLUSION

In this work, extending asymmetric modes in a LiNbO₃ thin film to higher orders is first theoretically studied for the purpose of scaling asymmetric mode resonances toward Ka band. Subsequently, a LiNbO₃ MEMS resonator with various resonances, the highest at 29.9 GHz, has been demonstrated for the first time. The developed MEMS resonator exhibits a k_t^2 of 0.94%, a measured overall Q_o of 328, and an extracted mechanical Q of 474 at 29.9 GHz. Further development and optimization of LiNbO₃ asymmetric resonators could lead to miniature Ka-band acoustic front-end filter technology that is currently unavailable for 5G.

REFERENCES

- [1] Federal Communications Commission, "Spectrum frontiers report and order and further notice of proposed rulemaking: FCC16-89," Jul. 2016. [Online]. Available: https://apps.fcc.gov/edocs_public/attachmatch/FCC-16-89A1.Rcd.pdf.
- [2] HUAWEI, "5G Spectrum Public Policy Position," 2018.
- [3] M. Hara, *et al.*, "Super-High-Frequency band filters configured with Air-Gap-Type Thin-Film Bulk Acoustic Resonators," *Jpn. J. Appl. Phys.*, Part 1 49, 07HD13 (2010).
- [4] S. Ballandras, *et al.*, "High overtone Bulk Acoustic Resonators: application to resonators, filters and sensors," *Acoustics Nantes, France*, 2012, pp.23-27.
- [5] R. Lu and S. Gong, "Study of Thermal Nonlinearity in Lithium Niobate Based MEMS Resonators," *Solid-State Sensors, Actuators Microsystems Conf. (TRANSDUCERS)*, 2015 18th Int., Jun. 2015.
- [6] S. Gong and G. Piazza, "Figure-of-merit enhancement for laterally vibrating lithium niobate MEMS resonators," *IEEE Trans. Electron Devices*, vol. 60, no. 11, pp. 3888-3894, Nov 2013.
- [7] R. H. Olsson III, K. Hattar, M. S. Baker, M. Wiwi, J. Nguyen, C. Padilla, S. J. Homeijer, J. R. Wendt, T. A. Friedmann, "Lamb wave micromechanical resonators formed in thin plates of lithium niobate", *Hilton head solid-state sensors, actuators and microsystems workshop*, 2014, pp 281-284
- [8] M. Kadota, T. Ogami, K. Yamamoto, H. Tochishita and Y. Negora, "High-Frequency Lamb Wave Device Composed of MEMS Structure Using LiNbO₃ Thin Film and Air Gap," *IEEE Trans. Ultrason. Ferroelectr. Freq. Control*, vol. 57, no. 11, NOV 2010.
- [9] Y. Yang, A. Gao, R. Lu, and S. Gong, "5 GHz lithium niobate MEMS resonators with high FoM of 153," *2017 IEEE 30th Int. Conf. on MEMS, Las Vegas, NV*, 2017, pp. 942-945.
- [10] Y. Yang, R. Lu, T. Manzanque, and S. Gong, "1.7 GHz Y-cut Lithium niobate MEMS resonators with FoM of 336 and $f \cdot Q$ of 9.15×10^{12} ," in *Microwave Symposim (IMS), 2018 IEEE MTT-S International*, 2018, pp. 1-4.
- [11] D. Royer and E. Dieulesaint (1996) *Elastic waves in Solids I free and guided propagation*. Springer, Paris.
- [12] R. Lu, T. Manzanque, Y. Yang, A. Kourani, and S. Gong, "Lithium niobate lateral overtone resonators for low power frequency-hopping applications," *2018 IEEE 31th Int. Conf. on MEMS, Belfast, Northern Ireland, UK*, 2018, pp. 751-754.
- [13] C. Cassella, G. Chen, Z. Qian, G. Hummel, and M. Rinaldi, "Aluminum nitride cross-sectional Lamé mode resonators," *J. Microelectromech. Syst.*, vol. 25, no. 2, pp. 275-285, Apr. 2015.
- [14] Y.-H. Song, R. Lu, and S. Gong, "Analysis and removal of spurious response in SH0 lithium niobate MEMS resonators," *IEEE Trans. Electron Devices*, vol. 63, no. 5, pp. 2066-2073, May 2016.
- [15] Hashimoto K (2009) *RF bulk acoustic wave filters for communications*. Artech House, Norwood, MA.